Available online at www.sciencedirect.com

ScienceDirect

Procedia Structural Integrity 42 (2022) 1215–1222

Structural Integrity Procedia

www.elsevier.com/locate/procedia

23 European Conference on Fracture - ECF23

Improving the understanding of how biaxiality ratios correlate on cruciform fatigue test specimens for VHCF ultrasonic fatigue testing

Diogo Montalvão[a,*], Kadir Hekim[a], Pedro Costa[b], Luís Reis[b], Manuel Freitas[b]

[a]*1Department of Design and Engineering, Faculty of Science and Technology, Bournemouth University, Poole House, Talbot Campus, Fern Barrow, Poole BH12 5BB, United Kingdom*

[b]*IDMEC, Department of Mechanical Engineering, Instituto Superior Técnico, University of Lisbon, Av. Rovisco Pais, 1, 1050-099 Lisboa, Portugal*

Abstract

Very High Cycle Fatigue (VHCF) using ultrasonic machines is a subject that is receiving growing attention. Recent developments focus on biaxial stresses which are of interest to industries such as the aeronautical where plane stresses appear in the fuselage and wings. It has been shown before that in-plane cruciform specimens can be changed so that different biaxiality ratios are achieved from equibiaxial to pure shear. This paper analyses how these biaxiality ratios relate to one another between the in-plane orthogonal directions x and y in cruciform specimens. Specimens in this study are composed of Aluminum 6082-T651, a medium strength alloy used in many highly stressed engineering applications, including trusses, cranes, bridges, and transportation. These asymmetric models are purposely designed to develop orthogonal biaxial stresses with non-unitary biaxiality ratios. Comparing the simulation results with the experimental data shows that the strain rates can provide acceptable prediction of biaxiality ratios. Moreover, it was observed that the biaxiality ratios obtained from stress, displacement and strain are not equal and, in fact, can be correlated by an expression that was derived during this research.

Keywords: Type your keywords here, separated by semicolons ;

* Corresponding author. Tel.: +44 (0) 1202 965 515
E-mail address: dmontalvao@bournemouth.ac.uk

10.1016/j.prostr.2022.12.155

1. Introduction

Most of the existing test equipment in the market for both classical and VHCF are uniaxial test machines (Lage et al., 2014), in the sense that the state of stress created is unidirectional. However, critical components used by the aerospace, automotive, energy, naval, medical, space and other industries are usually subjected to complex multiaxial loading conditions (Bathias, 2006 and Freitas et al., 2014). Typical biaxial in-plane fatigue machines require that the centre of the specimen does not move during the test, meaning that the actuators (usually four) must be precisely synchronised (Freitas et al. 2014 and Baptista et al., 2014). Furthermore, the almost only available in-plane biaxial machines available so far in the market use servo-hydraulic actuators. Thus, these machines are not good candidates to be used in VHCF.

For biaxial fatigue testing, there are currently two methods of producing biaxial stresses in material for different types of specimens (Freitas, 2017). The first method employs thin-walled cylinder tube specimen subjected to combined tension–torsion loading, whereas the second method uses cruciform specimens subjected to the biaxial tension-tension loadings. Fig. 1 represents schematically the range of biaxial principal stress states, σ_1 and σ_2, in the four quadrants. It shows the range of possible combination of stresses, from in-plane biaxial stress states in the first and third quadrants to the presence of shear stresses in the second and fourth quadrants.

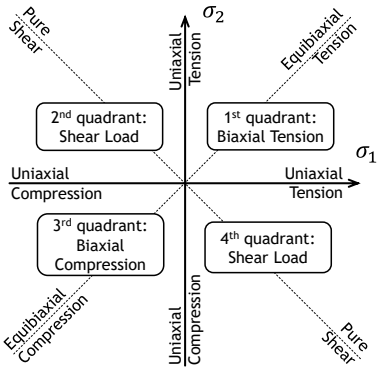

Fig. 1. Schematic representation of biaxial stress states (based in Freitas, 2017).

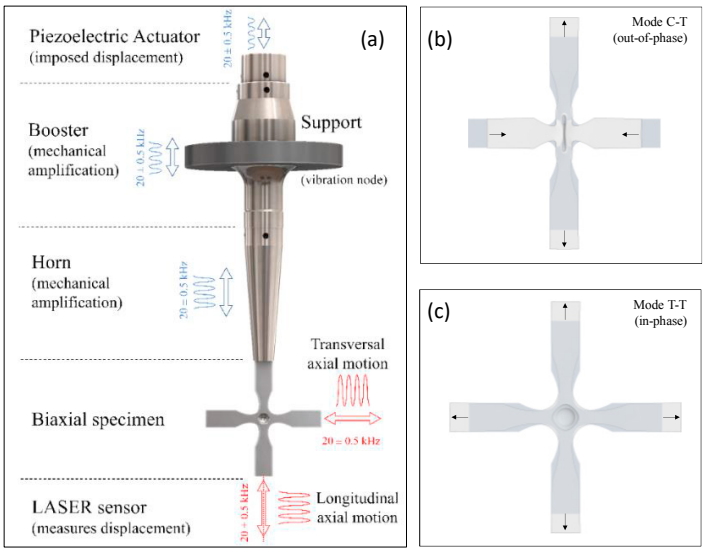

Fig. 2. (a) VHCF testing machine resonant system components with biaxial specimen; (b) CT (pure shear, out-of-phase) mode shape with $B = -1$; (c) TT (equibiaxial, in-phase) mode shape with $B = 1$ (Montalvão and Wren, 2017 and Costa et al., 2020).

Montalvão and Wren (2017) and Costa et al. (2019) proposed an original approach to biaxial fatigue testing in the VHCF regimen (Fig. 2 (a)). Having as a starting point the same principles used in the design of VHCF machines and UFT specimens as Bathias (2006), Lage et al. (2014), and Baptista et al. (2014, 2015) it was shown that, at least when using cruciform specimens for in-plane axial-axial (biaxial) testing, only the specimen needs to be redesigned. No changes are required to be made to the machine are required as, for example, in a work where combined axial-torsion is obtained (Costa et al., 2017). Based on those design principles, Montalvão et al. (2019) developed test specimens that can deliver biaxiality ratios $B \in [-1, 1]$, i.e., that can produce any ratio between the biaxial principal stress states (Fig. 1), σ_1 and σ_2, ranging from pure shear ($B = -1$) to equibiaxial ($B = 1$) (Fig. 2 (b)). When the biaxiality ratio is determined from two orthogonal stresses in the x and y directions, the biaxiality ratio is defined as:

$$B_\sigma = \begin{cases} \sigma_y/\sigma_x & if \ \ |\sigma_x| \geq |\sigma_y| \\ \sigma_x/\sigma_y & if \ \ |\sigma_x| < |\sigma_y| \end{cases} \quad (1)$$

which can be written in the simpler form:

$$B_\sigma = \left(\frac{\sigma_x}{\sigma_y}\right)^{sgn\,(|\sigma_y|-|\sigma_x|)} \quad (2)$$

This means that for $B = \pm 1$ we have the same in-plane stresses in both directions (symmetric cruciform specimens) and for the limit case where $B = 0$ we have uniaxial stress in one direction only. The signal is indicating if the mode shape is either in-phase (TT, or Tension-Tension) when positive (+), or out-of-phase (CT, or Compression-Tension) when negative (-).

When biaxiality ratios $B \neq \pm 1$ are being sought, the non-unitary biaxiality ratio can be achieved by changing the arms' lengths in different directions by different proportions (Fig. 4) (Montalvão et al., 2019). If the arm in the horizontal direction is shortened by a quantity $-\Delta x$, this corresponds to a reduction in the mass in the horizontal direction; hence, to an increase in the natural frequency. To compensate for this increase in the natural frequency, the arm in the vertical direction is extended by a quantity $+\Delta y$ until the frequency is reduced back to 20 kHz. Fig. 3 shows one example of what a specimen with a non-unitary biaxiality ratio may look like following this procedure.

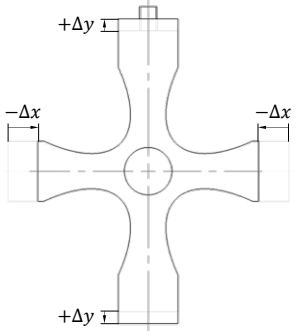

Fig. 3. Result from the "change in arms' dimensions" method to obtain an out-of-phase CT specimen with a non-unitary biaxiality ratio at 20 kHz (Montalvão et al., 2019).

In this paper, the authors further investigate these non-symmetrical cruciform specimens used to generate non-unitary biaxiality ratios through Finite Element Analysis (FEA). Results show that one cannot define a single biaxiality ratio when it comes to dynamic specimens, but rather that there are three (or four) biaxiality ratios to be considered: strain biaxiality ratio B_ε, stress biaxiality ratio B_σ, displacement biaxiality ratio B_d, and 'design' biaxiality ratio B_Δ (i.e., a biaxiality ratio that is based in the dimensional change in arms' lengths). Furthermore, it is shown that these ratios are not independent from one another and that they can be correlated with an expression that was empirically determined, which is at least valid for CT specimens (i.e., where $B < 0$). This relation is an important result that is important for both future research in this field and application of the methods by industry.

2. Background Principles

2.1. Biaxiality ratios definitions

The specimens used in this study are based on the ones proposed by Montalvão et al. (2019), made from Aluminum 6082-T651. This is a medium strength alloy with a fibrous core microstructure that is heat treatable and have high corrosion resistance rate. It is used in many highly stressed engineering applications, including trusses, cranes, bridges, and transportation. It also has excellent extrudability which helps in the manufacturing and machining of the specimens.

In this paper, specimens described by Montalvão et al. (2019) were analysed, where the biaxiality ratio B_Δ (the 'design' ratio) was initially defined as the ratio between the changes in the arms lengths (Fig. 4), i.e.:

$$B_\Delta = \left(\frac{\Delta_x}{\Delta_y}\right)^{sgn\,(|\Delta_y|-|\Delta_x|)} \tag{3}$$

In the work from Montalvão et al. (2019) it was assumed that the biaxiality ratios would only differ slightly no matter if strains, stresses, changes in arms lengths or displacements at the tips were used. Small changes were attributed to the fact that the rectangular tips of the specimens are not lump masses (as the design model assumes): they also deform elastically, although this is much less relevant than what is happening closer to the specimen's centre where the width and thickness change. be the same. However, and as it will be shown with this work, more in-depth analysis shows that this is not true. If we now define the two missing biaxiality ratios:

$$B_\varepsilon = \left(\frac{\varepsilon_x}{\varepsilon_y}\right)^{sgn\,(|\varepsilon_y|-|\varepsilon_x|)} \tag{4}$$

$$B_d = \left(\frac{d_x}{d_y}\right)^{sgn\,(|d_y|-|d_x|)} \tag{5}$$

where ε_x and ε_y are the strains at the centre of the specimen in the x and y directions, respectively, and d_x and d_y are the displacements at the tips of the specimens in the x and y directions, respectively, then what we will observe is:

$$B_\sigma \neq B_\varepsilon \neq B_d \tag{6}$$

$$B_d = B_\Delta \tag{7}$$

Therefore, the underlying question is: How can non-unitary cruciform biaxial specimens be designed so that they deliver a determined B_σ (or B_ε) when the design variables (i.e., geometrical dimensions) are based on B_Δ instead? Is there any relationship between them? That is what we will find out in this paper.

2.2. Hooke's law

We need to go back to first principles to understand why the biaxiality ratios B_σ, B_ε and B_d differ between them. Without going into details, as any textbook on mechanics of materials will show, Hooke's law for a linear elastic isotropic material can be defined as:

$$\begin{cases} \sigma_x = \frac{E}{(1+\upsilon)(1-2\upsilon)}\left[(1-\upsilon)\varepsilon_x + \upsilon\left(\varepsilon_y + \varepsilon_z\right)\right] \\ \sigma_y = \frac{E}{(1+\upsilon)(1-2\upsilon)}\left[(1-\upsilon)\varepsilon_y + \upsilon(\varepsilon_x + \varepsilon_z)\right] \\ \sigma_z = \frac{E}{(1+\upsilon)(1-2\upsilon)}\left[(1-\upsilon)\varepsilon_z + \upsilon\left(\varepsilon_x + \varepsilon_y\right)\right] \end{cases} \quad (8)$$

$$\begin{cases} \varepsilon_x = \frac{1}{E}\left[\sigma_x - \upsilon\left(\sigma_y + \sigma_z\right)\right] \\ \varepsilon_y = \frac{1}{E}\left[\sigma_y - \upsilon(\sigma_x + \sigma_z)\right] \\ \varepsilon_z = \frac{1}{E}\left[\sigma_z - \upsilon\left(\sigma_x + \sigma_y\right)\right] \end{cases} \quad (9)$$

Cruciform test specimens are moderately thin throughout, with a considerably thinner central area (Fig. 4). Maximum stresses and strains will occur at the centre, where will have a situation of plane stress with $\sigma_z \simeq 0$ and $\varepsilon_z \neq 0$. In other words, stresses develop in the xy plane only, but strains are developing in all three cartesian directions, so it is not difficult to understand that B_σ does not necessarily has to be equal to B_ε.

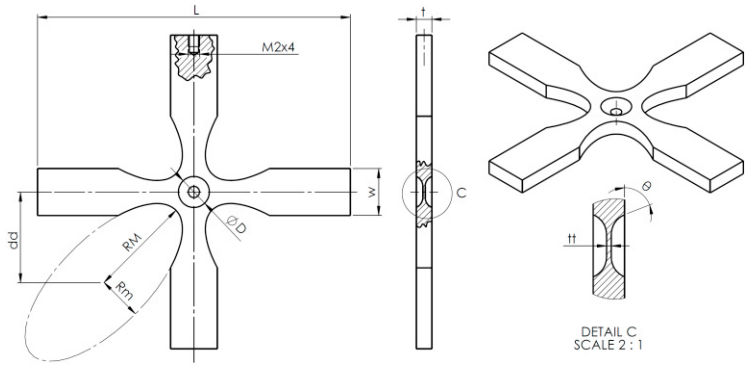

Fig. 4. Cruciform test specimen's general drawing (Montalvão and Wren, 2017) (symmetric equibiaxial case for illustration purposes only).

3. Methodology

To better understand how the 4 biaxiality ratios B_σ, B_ε, B_d and B_Δ change and compare with each another, Hooke's law equations (8) and (9) are used, as well as Finite Element Analysis (FEA) using ANSYS Workbench 2021 R2. Initially, specimens are modelled in free-free configuration and a simulation of the type Modal is run. The objective is to slightly adjust dimensions so that specimens are tuned to have either a CT or a TT mode shape at 20±0.5 kHz, which is the operational range available at the machine's at both the University of Lisbon in Portugal and the ADDISONIC lab at Bournemouth University in the UK. Similar simulations are then run but with the specimen assembled at the machine, as depicted in Fig. 2, to have a better representation of reality and further refine the specimens' design.

Hex dominant elements were used with attention to distortion of the elements to produce results with an acceptable level of accuracy. This was determined after mesh convergence was achieved when refining both the global mesh and local mesh at the centre.

The relation between displacements at the tips of the specimen and stress and strain at the centre, which is needed in the case of experimental testing as stress and strain are monitored from the displacement at the tips from a contactless laser sensor, is determined from a simulation of the type Harmonic (used to get the frequency response functions). Excitation forces of 0.25N, 0.5N and 1N were applied to the model at one of the anti-nodes (i.e., specimen's tips). The different excitation forces were used to assess the system's response against increasing loading conditions. Three different loads were used to check linearity of the model. The analyses settings are set up to test the specimen at the exact value of the natural frequency in the vicinity of 20 kHz.

In this paper, three of the asymmetric specimens described by Montalvão et al. (2019) were analysed (table 1). The reason why CT and TT specimens with biaxiality ratios ranging from $B_\Delta = \pm 0.40$ to $B_\Delta = \pm 0.77$ were chosen, is because these biaxiality ratios are well set apart from each other and somewhat *extreme* in terms of dimensions (especially for $B_\Delta = \pm 0.40$ where substantial dimensional changes are required). However, any other specimens could have been chosen and should not condition the findings of this study. The geometry is based on a cruciform configuration, featuring corner elliptical fillets between the specimen's arms, to reduce stress concentrations and to maximise stress at the specimen's centre (Baptista et al., 2014, 2015).

Table 1. Changes in arms' lengths and biaxiality ratios for specimens with non-unitary biaxiality ratios analysed in this study.

Specimens type CT (shear, out-of-phase)				Specimens type TT (biaxial, in-phase)			
Model	Δx (mm)	Δy (mm)	B_Δ	Model	Δy (mm)	Δx (mm)	B_Δ
CT.77	1.5	-1.95	-0.77	TT.77	2	-1.55	0.77
CT.62	2.5	-4.05	-0.62	TT.62	4	-2.5	0.62
CT.40	4	-10.1	-0.40	TT.40	10	-4	0.40

4. Results and Analysis

FEA was used to determine the stresses, strains, and displacements in the 3 cartesian directions x, y, and z. Results are shown in table 2. Hooke's law was used to validate results (i.e., determine stresses from FEA strains and vice versa) which were found to be correct.

Table 2. Stress, strain, and displacement at tips FEA results for both the CT and TT specimens with different 'design' biaxiality ratios.

	σ_x (MPa)	σ_y (MPa)	σ_z (MPa)	ε_x	ε_y	ε_z	d_x (mm)	d_y (mm)
CT.40	119	-221	1.1	2.67E-03	-3.61E-03	4.57E-04	1.75E-02	-4.35E-02
CT.62	218	-301	0.6	4.41E-03	-5.17E-03	3.74E-04	3.53E-02	-5.70E-02
CT.77	283	-337	1.1	5.47E-03	-5.98E-03	2.41E-04	4.80E-02	-6.23E-02
CT.100	366	-365	0.7	6.76E-03	-6.75E-03	1.21E-05	6.47E-02	-6.47E-02
TT.40	414	72	3.4	5.40E-03	-9.14E-04	-2.18E-03	9.57E-02	3.84E-02
TT.62	321	144	3.2	3.78E-03	5.20E-04	-2.09E-03	7.85E-02	4.87E-02
TT.77	267	175	3.1	2.90E-03	1.20E-03	-1.99E-03	6.82E-02	5.27E-02
TT.100	198	198	2.7	1.83E-03	1.83E-03	-1.80E-03	5.41E-02	5.41E-02

With this data, the B_σ, B_ε and B_d biaxiality ratios can now be determined, which results are shown in table 3.

Table 3. Biaxiality ratios B_σ, B_ε and B_d for both CT and TT specimens with different 'design' biaxiality ratios.

	B_σ	B_ε	$B_d(=B_\Delta)$	$B_\sigma \times B_\varepsilon$		B_σ	B_ε	$B_d(=B_\Delta)$	$B_\sigma \times B_\varepsilon$
CT.40	-0.54	-0.74	-0.40	0.40	TT.40	0.17	-0.17	0.40	-0.03
CT.62	-0.72	-0.85	-0.62	0.62	TT.62	0.45	0.14	0.62	0.06
CT.77	-0.84	-0.92	-0.77	0.77	TT.77	0.66	0.41	0.77	0.27
CT.100	-1.00	-1.00	-1.00	1.00	TT.100	1.00	1.00	1.00	1.00

The first aspect to notice from table 3 is that $B_d = B_\Delta$. This is important because when using machines such as the one shown in figure 16 where the displacement at the tips is measured from a laser, the 'design' biaxiality ratio B_Δ can be validated. On the other hand, and as it was noted before, that $B_\sigma \neq B_\varepsilon \neq B_d$.

However, what is more interesting to note from the observation of tables 2 and 3, is that if we take the product between the stress biaxiality ration and the strain biaxiality ratio the following is obtained:

$$\left|B_{\sigma,CT} \times B_{\varepsilon,CT}\right| = \left|B_{\Delta,CT}\right| \tag{10}$$

$$\left|B_{\sigma,TT} \times B_{\varepsilon,TT}\right| \neq \left|B_{\Delta,TT}\right| \tag{11}$$

FEA analysis can be used to better understand what is happening. Let us take as an example specimen TT.40 (Fig. 5). Firstly, the deformation of non-unitary TT specimens is harder to predict, as the motion due to the Poisson ratio in one direction is 'counteracted' by the motion in the same direction of the vibrating pattern. This will also induce high stresses at locations that are not intended, at the corners as shown in Fig. 5 (b), which could lead to the development of cracks at the corners rather than of developing from the centre. However, this does not still explain why for CT specimens $\left|\mathrm{B}_{\sigma,\mathrm{CT}} \times \mathrm{B}_{\varepsilon,\mathrm{CT}}\right| = \left|\mathrm{B}_{\Delta,\mathrm{CT}}\right|$ while for TT specimens this is not true, i.e., $\left|\mathrm{B}_{\sigma,\mathrm{TT}} \times \mathrm{B}_{\varepsilon,\mathrm{TT}}\right| \neq \left|\mathrm{B}_{\Delta,\mathrm{TT}}\right|$. If we now look at the deformation of the specimen in one direction, comparison of Fig. 5 (c) with Fig. 5 (d), shows that the deformation at the centre of the specimen is out-of-phase with the arms. This does not happen with CT specimens, as the movement of the arms follows the same direction as the deformation that would result from a positive Poisson's ratio.

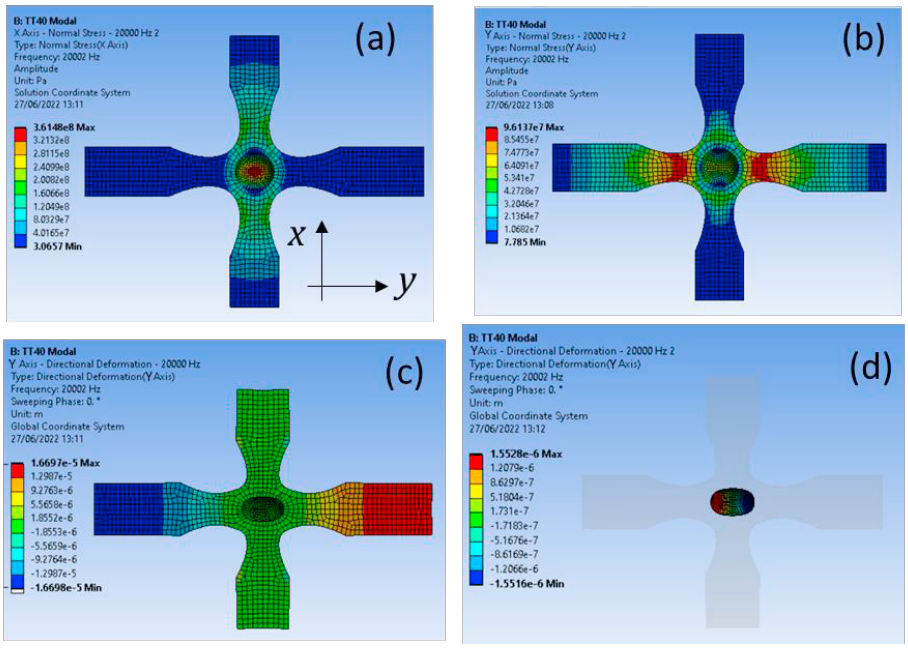

Fig. 5. FEA results using as an example TT.40 specimen: (a) σ_x, (b) σ_y, (c) d_y, (d) d_y close-up at the centre of the specimen.

If Hooke's law is taken into consideration, the product between the stress and strain biaxiality ratios (for plane stress) can be written as:

$$B_\sigma \times B_\varepsilon = \left[\frac{\sigma_x\varepsilon_x + \upsilon(\sigma_x\varepsilon_y - \sigma_y\varepsilon_x) - \upsilon^2\sigma_y\varepsilon_y}{\sigma_y\varepsilon_y + \upsilon(\sigma_y\varepsilon_x - \sigma_x\varepsilon_y) - \upsilon^2\sigma_x\varepsilon_x}\right]^{sgn(|\varepsilon_y| - |\varepsilon_x|)} \tag{12}$$

This equation was used to confirm the results presented in tables 2 and 3, showing that there are some challenges with the design of TT (biaxial, in-phase) specimens that do not seem to exist when CT specimens (shear, out-of-phase) are considered. Costa et al. (2019) already observed before and through experimental work problems with TT (equibiaxial) specimens which have further been highlighted with this work.

5. Conclusions

This paper analyses non-unitary biaxiality cruciform specimens that are designed for Ultrasonic Fatigue Testing (UFT) at 20 kHz. The results can be easily transferred to cruciform specimens that are not meant to be used in UFT testing machines, since the analysis relays on first principles. It is hoped that this paper will give insight to researchers and engineers who are interested in in-plane biaxial fatigue testing about the challenges (as well as advantages) with the use and design of such specimens. Notwithstanding, this paper also highlights that biaxiality ratios must be distinguished between stress, strain, and deformation, as they are not necessarily the same. Furthermore, it has been shown that, at least for CT specimens, they can be related with one another. Therefore, the designer can consider the newly presented relationship to ensure the stress or strain ratios being obtained at the centre of the specimen are as per the design intent. Finally, this paper demonstrates that further research is still required when it comes to the design of biaxial specimens for fatigue testing, but that they have the potential to be used to replicate a varied number of combinations of biaxiality ratios that could better replicate real life loading conditions.

Acknowledgements

The authors would like to thank Research England through Bournemouth University for financially supporting this research work. This work is also co-financed by the project PTDC/EME-EME/7678/2020, Giga-Cycle Fatigue Behaviour of Engineering Metallic Alloys.

References

Baptista, R., Claudio, R.A., Reis, L., Guelho, I., Freitas, M., Madeira, J.F.A., 2014. Design optimization of cruciform specimens for biaxial fatigue loading. Frattura Integrità Strutturale, 8, 118–126.

Baptista, R., Claudio, R.A., Reis, L., Madeira, J.F.A., Guelho, I., Freitas, M., 2015. Optimization of cruciform specimens for biaxial fatigue loading with direct multi search. Theoretical and Applied Fracture Mechanics, 80, 65–72.

Bathias, C. 2006. Piezoelectric fatigue testing machines and devices. International Journal of Fatigue, 28, 1438–1445.

Costa, P., Vieira, M., Reis, L., Ribeiro, A., de Freitas, M., 2017. New specimen and horn design for combined tension and torsion ultrasonic fatigue testing in the very high cycle fatigue regime. International Journal of Fatigue, 103, 248–257.

Costa, P.R., Montalvão, D., Freitas, M., Baxter, R., Reis, L., 2019. Cruciform specimens' experimental analysis in ultrasonic fatigue testing. Fatigue & Fracture of Engineering Materials and Structures, 42, 2496–2508.

Costa, P.R., Nwawe, R., Soares, H., Reis, L., Freitas, M., Chen, Y., Montalvão, D., 2020. Review of Multiaxial Testing for Very High Cycle Fatigue: From 'Conventional' To Ultrasonic Machines. Machines, 80, 25.

Freitas, M., Reis, L., Li, B., Guelho, I., Antunes, V., Maia, J., Cláudio, R., 2014. In-Plane Biaxial Fatigue Testing Machine Powered by Linear Iron-Core Motors. Journal of ASTM International: Selected Technical Papers on Application of Automation Technology in Fatigue and Fracture Testing and Analysis, 1571, 63-79.

Freitas, M., 2017. Multiaxial fatigue: From materials testing to life prediction. Theoretical and Appled Fracture Mechanics, 92, 360–372.

Lage, Y., Ribeiro, A., Montalvão, D., Reis, L., Freitas, M., 2014. Automation in strain and temperature control on VHCF with an ultrasonic testing facility. Journal of ASTM International: Selected Technical Papers on Application of Automation Technology in Fatigue and Fracture Testing and Analysis, 1571, 80-100.

Montalvão, D., Wren, A., 2017. Redesigning axial-axial (biaxial) cruciform specimens for very high cycle fatigue ultrasonic testing machines. Heliyon, 3, e00466.

Montalvão, D., Blaskovics, A., Costa, P., Reis, L., Freitas, M., 2019. Numerical analysis of VHCF cruciform test specimens with non-unitary biaxiality ratios. International Journal of Computational Methods and Experimental Measurements. 7, 327–339.